

**Highlighting research from the group of Prof. Wei Zhan  
of the Department of Chemistry and Biochemistry  
at Auburn University, USA.**

Dipolar Janus liposomes: formation, electrokinetic motion  
and self-assembly

Presented herein is the first report on dipolar Janus  
liposomes—liposomes that contain opposite surface charges  
decorating the two hemispheres of the same colloidal body.  
Microscopic evidence is given in regard to the formation,  
electrokinetic motion as well as electrostatic self-assembly  
behavior of these new Janus particles.

**As featured in:**



See Wei Zhan *et al.*,  
*Soft Matter*, 2020, **16**, 2177.



# Dipolar Janus liposomes: formation, electrokinetic motion and self-assembly†

Zening Liu, Jinyan Cui and Wei Zhan \*

Cite this: *Soft Matter*, 2020, **16**, 2177

Received 13th November 2019,  
Accepted 20th January 2020

DOI: 10.1039/c9sm02254f

rsc.li/soft-matter-journal

**Presented herein is the first report on dipolar Janus liposomes—liposomes that contain opposite surface charges decorating the two hemispheres of the same colloidal body. Such heterogeneous organization of surface charge is achieved through cholesterol-modulated lipid phase separation, which sorts anionic/cationic lipids into coexisting liquid-ordered/liquid-disordered domains. We present optimized experimental conditions to produce these liposomes in high yields, based on the gel-assisted hydration of ternary lipid systems consisting of cholesterol, 1,2-dipalmitoyl-*sn*-glycero-3-phosphocholine, and 1,2-dioleoyl-*sn*-glycero-3-phosphocholine. The size/charge distribution and domain configuration of these liposomes are characterized in detail by confocal fluorescence microscopy, nanosphere binding and zeta potential measurements. Using confocal fluorescence microscopy, we also follow the electrokinetic motion as well as the electrostatic self-assembly of these new dipolar Janus particles.**

## Introduction

Research into Janus particles<sup>1–3</sup> continues to advance apace, fueled in particular by the opportunities to discover novel properties promised by the broken symmetry and anisotropy in these heterogeneous colloids. Aided by precise polymer synthesis and surface engineering, this effort has produced a great variety of Janus particles with split surface chemistries.<sup>4–6</sup> For example, juxtaposing polar and hydrophobic motifs gives rise to surfactant-like colloidal particles,<sup>7,8</sup> and from positive/negative charges, giant electric dipoles.<sup>9,10</sup> By contrast, as a class of heterogeneous soft colloidal particles, Janus liposomes have received relatively little attention. Of the few studies that have appeared in the literature so far, Beales, Nam and Vanderlick reported in this journal in 2011 the first systematic study on giant Janus

liposomes, employing electroformed liposomes composed of DPPC/DOPC/cholesterol.<sup>11</sup> In a more recent study,<sup>12</sup> we demonstrated that giant Janus liposomes capable of regional bioaffinity binding<sup>13,14</sup> could also be produced in high yields through a gel-assisted hydration process. In both cases, DPPC and DOPC contained in the same liposomes segregate from each other due to their mismatched acyl chains, *i.e.*, the all-saturated dipalmitoyl chain of DPPC *vs.* the unsaturated dioleoyl of DOPC. Such mutual lipid exclusion leads to a global lipid phase separation in individual liposomes over time, in which cholesterol plays a critical role in maintaining the DPPC-enriched phase fluid at room temperature, *i.e.*, the *l<sub>o</sub>* phase. The DOPC-enriched *l<sub>d</sub>* phase is also fluid, but only so because its double bonds give rise to a higher degree of hydrocarbon chain motion and hence less ordered lipid packing.<sup>15–17</sup> It is these two immiscible<sup>18</sup> but coexisting liquid phases that render these liposomes their Janus configuration, a feature fundamentally distinctive from many other types of Janus particles.<sup>1–6</sup>

In the present study, we asked if opposite charges can be configured face-to-face on the same colloidal body to yield dipolar Janus liposomes (DJLs). Besides its fundamental interest, *e.g.*, in lipid-based colloid chemistry and self-assembly, this effort was also inspired by many attractive features demonstrated by solid/polymer Janus particles carrying heterogeneous surface charges. For example, Granick and coworkers prepared ammonium/carboxylic dipolar Janus particles through selective gold deposition on polystyrene microbeads followed by thiol self-assembled monolayer formation.<sup>10</sup> These dipolar Janus particles were found to form clusters of various shapes and sizes under low electrolyte conditions, which were well captured by Monte Carlo simulation. In another study, Nisisako and coworkers<sup>19</sup> prepared heterogeneously charged polyacrylate Janus micro-particles using a microfluidic setup. Exploiting the different charge levels and colors associated with the nanoparticles, they further demonstrated a black-and-white electrical display device using these Janus particles. As detailed below, the successful preparation of DJLs following lipid sorting is first confirmed by using charged fluorescent nanospheres to track charge location

Department of Chemistry and Biochemistry, Auburn University, Auburn, AL 36849, USA. E-mail: wzz0001@auburn.edu

† Electronic supplementary information (ESI) available. See DOI: 10.1039/c9sm02254f

on liposomes. Similar to their solid/polymeric counterparts, these DJLs can also self-assemble electrostatically into more complex clusters. The dipolar charge configuration in these Janus liposomes is further confirmed by their distinctive electrokinetic motion behavior.

## Results and discussion

### Design and formation of dipolar Janus liposomes (DJLs)

We set out to build DJLs with the DPPC/DOPC/cholesterol ternary system because its liquid–liquid coexistence state can be accessed in a relatively broad range of lipid compositions at room temperature.<sup>16,17</sup> To configure these Janus liposomes with a dipolar charge arrangement, we in addition incorporate anionic 1,2-dipalmitoyl-*sn*-glycero-3-phospho-(1'-*rac*-glycerol) (sodium salt) (DPPG) and cationic 1,2-dioleoyl-3-trimethylammonium-propane (chloride salt) (DOTAP) into the formation. While DPPG is naturally occurring, *e.g.*, as a major lung surfactant component,<sup>20</sup> DOTAP is a synthetic cationic lipid frequently used in gene transfection and delivery<sup>21</sup> through electrostatic complexation with DNAs and RNAs. Both lipids, in addition, are expected to be highly charged in water, as the  $pK_a$  of DPPG<sup>22</sup> is  $\sim 1$  and DOTAP is a quaternary ammonium cation. As before, we hypothesize that these two charged lipids can be sorted into the two liquid lipid domains according to their acyl chains, that is, the DPPG into DPPC-enriched  $l_o$  domain and the DOTAP into DOPC-enriched  $l_d$  domain. Finally, in order to examine these liposome products with fluorescence microscopy, lipid phase indicator dyes, Rho-DOPE ( $l_d$ , red) and Bodipy-chol ( $l_o$ , green), were also included in the formation. A full description of the liposome formation procedure is given in the ESI.†

We started with liposome products composed of 35/35/30 DPPC/DOPC/cholesterol (mole ratio), which, as we found previously, yielded mostly Janus liposomes with roughly even-split  $l_o/l_d$  domains.<sup>12</sup> When 2% DPPG and DOTAP each were added into the lipid precursor, spherical liposomes could still be produced, but they seldom reached a satisfactory level of global phase separation (ESI,† Fig. S1). This negative but interesting result can be understood on the grounds of electrostatic interactions emanating from these charged lipids, which discourage phase separation (which acts to pull attracting DPPG and DOTAP apart) on one hand, and raise the kinetic barrier for merging among small  $l_d$  domains (each now bearing like charge) on the other. To counterbalance such electrostatic interactions so that the lipid coalescence can proceed unhindered, we increased the share of DPPC/DOPC stepwise in the lipid makeup at the expense of cholesterol, while keeping the charge loading constant (ESI,† Fig. S1). Iteration as such then led us to the composition of DPPC/DOPC/cholesterol/DPPG/DOTAP mixed at 38/38/20/2/2 mole ratio, which produces Janus liposomes at a high yield of  $\sim 80\%$  (Fig. 1a). Moreover, the majority of the giant liposomes thus formed have diameters in the range of 5–20  $\mu\text{m}$  (Fig. 1b). On average, these liposomes contain in their structures a smaller  $l_o$  domain, *i.e.*, 46% vs. 54% associated with the  $l_d$  domain (Fig. 1b inset). Thus, we have achieved our first goal of this

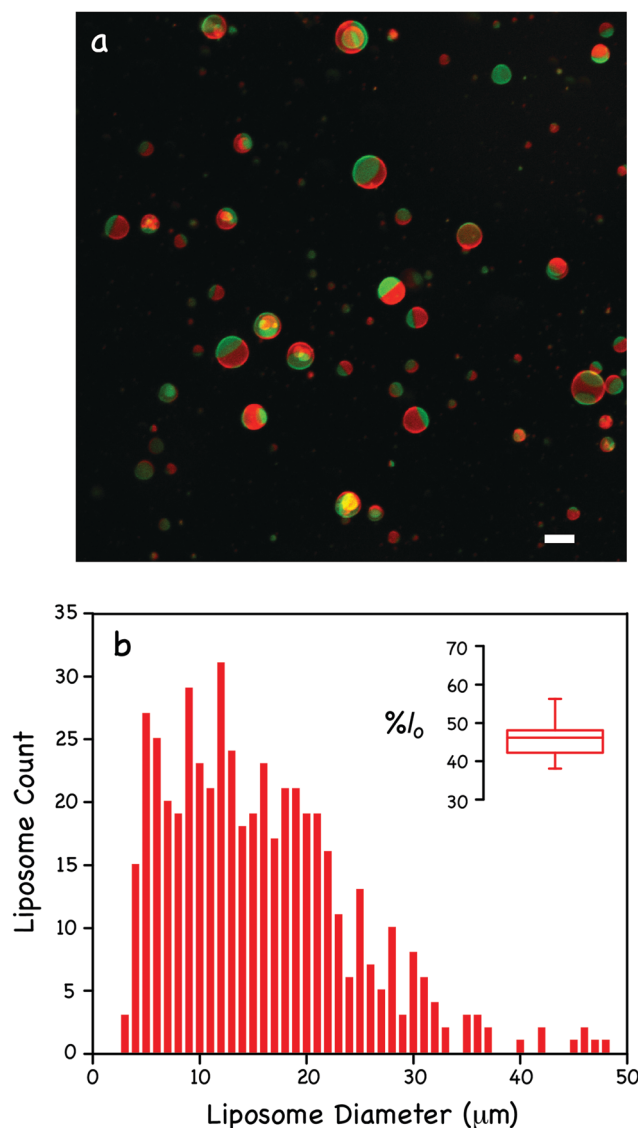


Fig. 1 (a) Fluorescence micrograph of liposomes freshly formed from a lipid precursor of DPPC/DOPC/Chol/DPPG/DOTAP/Bodipy-chol/Rho-DOPE mixed at 38/38/20/2/2/0.2/0.2 mole ratio; the total lipid concentration in the final liposome product is  $\sim 5 \mu\text{M}$ . Scale bar: 10  $\mu\text{m}$ . (b) Size distribution of dual-charged Janus liposomes ( $n = 500$ ). The liposome diameter is determined from fluorescence micrographs similar to (a) and reported to the closest micrometers. Inset: Percent area occupied by the liquid-ordered hemisphere ( $\%l_o$ ) in dual-charged Janus liposomes ( $n = 100$ ).

investigation – a lipid formula that contains both anionic and cationic lipids and at the same time still affords good Janus liposome formation.

### Charge placement in liposomes

We moved next onto the identification of DPPG/DOTAP distribution in these Janus liposomes. To do so, we employed fluorescent polystyrene (PS) nanospheres whose surfaces are terminated with either  $-\text{COOH}$  or  $-\text{NH}_2$  groups (see the ESI† for more detail). Through electrostatic binding, these charged fluorescent particles are expected to coat the surface of Janus liposomes and thus reveal the location of charged lipids in the



**Table 1** Zeta potential ( $\zeta$ ) values of aqueous-suspended Janus liposomes and polystyrene (PS) nanospheres

Sample	$\zeta$ (mV)	Sample	$\zeta$ (mV)
<b>Zwitterionic</b>		<b>Dipolar</b>	
Unlabeled <sup>a</sup>	$-2.5 \pm 0.2^i$	Unlabeled <sup>d</sup>	$9.1 \pm 1.2^i$
<i>l</i> <sub>d</sub> -Labeled <sup>b</sup>	$-5.7 \pm 0.2^i$	<i>l</i> <sub>d</sub> -Labeled <sup>e</sup>	$2.5 \pm 0.6^i$
Dual-labeled <sup>c</sup>	$-4.4 \pm 0.3^i$	Dual-labeled <sup>f</sup>	$5.2 \pm 0.7^i$
<b>PS nanospheres</b>		<b>Monopolar</b>	
-COOH	$-42.6 \pm 0.4^i$	(-), dual-labeled <sup>g</sup>	$-19.1 \pm 0.8^i$
-NH <sub>2</sub>	$18.4 \pm 1.0^i$	(+), dual-labeled <sup>h</sup>	$18.7 \pm 0.4^i$

<sup>a</sup> DPPC/DOPC/Chol = 40:40:20 (mol%). <sup>b</sup> Composition as in *a* plus 0.2 mol% Rho-DOPE. <sup>c</sup> Composition as in *a* plus 0.2 mol% Rho-DOPE and Bodipy-chol each. <sup>d</sup> DPPC/DOPC/Chol/DPPG/DOTAP = 38:38:20:2:2. <sup>e</sup> Composition as in *d* plus 0.2 mol% Rho-DOPE. <sup>f</sup> Composition as in *d* plus 0.2 mol% Rho-DOPE and Bodipy-chol each. <sup>g</sup> DPPC/DOPC/Chol/DPPG/Rho-DOPE/Bodipy-chol = 38:40:20:2:0.2:0.2. <sup>h</sup> DPPC/DOPC/Chol/DOTAP/Rho-DOPE/Bodipy-chol = 40:38:20:2:0.2:0.2. <sup>i</sup> Standard deviation ( $n = 5$ ).

latter. The zeta potentials of these nanospheres are included in Table 1.

As shown in Fig. 2, green fluorescent nanospheres bind these dual-charged liposomes in a domain-specific fashion, *i.e.*, PS-COOH to the *l*<sub>o</sub> domain and PS-NH<sub>2</sub> to the *l*<sub>d</sub> domain, in accordance with the designated placement of DPPG (*l*<sub>o</sub>) and DOTAP (*l*<sub>d</sub>). Here, an interesting distinction can be made between the two charged lipids. While dotted nanosphere attachments are detected in both cases upon overnight incubation (Fig. 2a and c), the binding between PS-COOH and the positively-charged *l*<sub>d</sub> domain clearly proceeds further. This, for example, produces an even, half-moon shaped nanosphere layer covering the *l*<sub>d</sub> domain after 3 days (Fig. 2b). By contrast, no such full coverages were seen when PS-NH<sub>2</sub> nanospheres were used instead (Fig. 2d). A similar trend was also observed when plain (unlabeled) liposomes were incubated with these charged

nanospheres (Fig. 2e–h), thus ruling out the possibility of fluorescent dyes being responsible for the observed formations. On the other hand, no nanosphere binding was detected when Janus liposomes free of DPPG/DOTAP were tested (data not shown). Taken together, these results confirm the domain-associated distribution of opposite charges in Janus liposomes, and hence the successful formation of the intended DJLs.

### Zeta potential measurement of DJLs

To further characterize the charge distribution in these DJLs, zeta potential measurement was carried out next. As summarized in Table 1, Janus liposomes comprising DPPC/DOPC/cholesterol display a slightly negative zeta potential of  $-2.5$  mV. While there exists no published zeta potential data on Janus liposomes, this number is within the range of reported values<sup>23,24</sup> for homogeneous zwitterionic liposomes containing cholesterol. Furthermore, when the *l*<sub>d</sub>-domain indicator dye, Rho-DOPE, was included in the sample at a 0.2% level, the zeta potential became more negative,  $-5.7$  mV, apparently due to its intrinsic negative charge. In contrast, the *l*<sub>o</sub>-domain indicator, Bodipy-chol, was found to modify the zeta potential toward more positive values, though to a lower extent compared to Rho-DOPE ( $-4.4$  mV). For charge-loaded samples, we found Janus liposomes singly charged with 2% DPPG or DOTAP (together with both dyes) to yield zeta potentials of comparable magnitude ( $-19.1$  mV *vs.*  $18.7$  mV). Finally, for DJLs that included both DPPG and DOTAP (again with both dyes present), a positive zeta potential of  $5.2$  mV was recorded.

### Electrokinetic motion of DJLs

To corroborate the above zeta potential data, which measure the collective electrophoretic behavior of liposome populations,

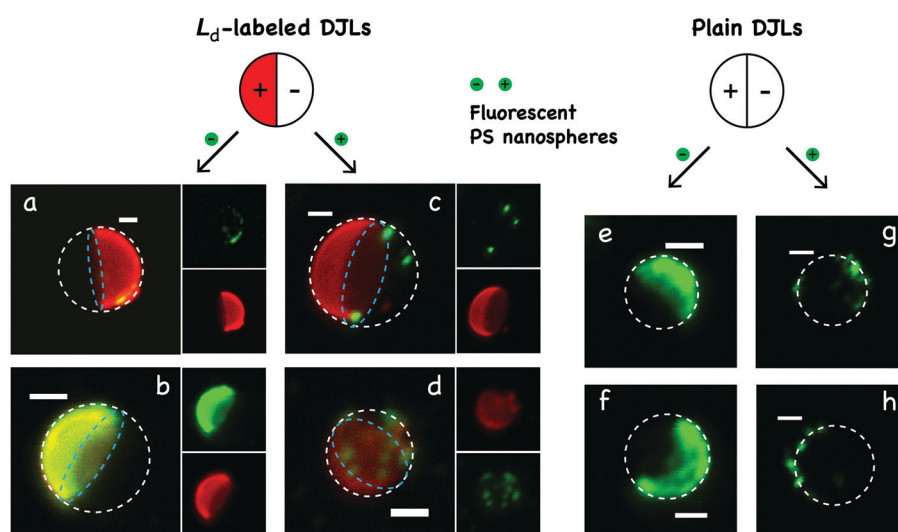


**Fig. 2** Placement of charged lipids in Janus liposomes as revealed by fluorescent polystyrene (PS) nanosphere binding. (left) Fluorescence micrographs of dual-charged, Rho-DOPE-labeled Janus liposomes upon incubation with either PS-COOH nanospheres (a and b) or PS-NH<sub>2</sub> nanospheres (c and d). Broken circles in white and blue outline the estimated circumference and phase boundary of the liposomes, respectively. Each liposome sample is shown by three images, one by dual (the image on the left) and the other two by single-channel excitation. Images (a and c) were acquired after overnight liposome/nanosphere incubation, whereas (b and d) were obtained after 3-day incubation. (Right) Fluorescence micrographs of unlabeled, dual-charged Janus liposomes upon binding with either PS-COOH nanospheres (images e and f) or PS-NH<sub>2</sub> nanospheres (images g and h) after 3-day incubation. Broken circles are added in the images as a visual guide of the liposome contour. Scale bars in all images represent  $5 \mu\text{m}$ .

we also monitored the electrokinetic motion of individual Janus liposomes subjected to a DC field. As described in the ESI,<sup>†</sup> this was carried out in linear microchannels made of cyclic olefin copolymers, which are known to sustain significant cathodic electroosmotic flow (EOF).<sup>25</sup> Since the liposome solution is confined in the microchannel, which sustains no net fluid flow across, a counter flow develops at the center of the microchannel to balance out the surface-originated EOF running in the opposite direction.<sup>26,27</sup> As shown in Fig. S3 and ESI<sup>†</sup> movies, this counter flow dominates the fluid movement at and near the midplane of the channel, carrying both zwitterionic and dipolar Janus liposomes toward the anode. Concurrent to migration, interestingly, both types of liposomes also undergo rotation. While the rotation of these liposomes does not follow any particular ordered sequence – due to their random initial orientations, it always acts to align the two hemispheres of these liposomes along the electric field.

Upon close inspection, however, several distinctive features between the two liposomes can be identified. (1) Terminal liposome orientation. In the case of DJLs, the  $l_o(-)$  domain always points to the anode and the  $l_d(+)$  domain points to the cathode, thus behaving like a giant electric dipole in a DC field. While not as highly loaded as DJLs, charge is nevertheless unevenly distributed between the two hemispheres of zwitterionic Janus liposomes, mainly due to the negatively-charged rhodamine residing in the  $l_d$  domain, which preferentially points to the anode (Fig. 3). Once aligned, both liposomes rotate no further and thereafter migrate onward with their respective fixed orientations. In other words, the rotation of these liposomes only occurs at the beginning of their electrokinetic motion, when their charged domain(s) are not yet fully aligned with the electric field. (2) Alignment time. In general, it takes less time for DJLs to achieve their steady terminal orientation, *e.g.*,  $\sim 20$  s as compared to  $\sim 40$  s observed for the zwitterionic liposome (Fig. 3). This makes sense – with their

higher charge level and dipolar charge distribution, DJLs experience a stronger electrostatic torque when not aligned with the external field than the zwitterionic liposome – under otherwise comparable conditions. (3) Electrokinetic mobility. While both types of liposomes migrate toward the anode, DJLs consistently register a lower mobility:  $2.2 \pm 0.5 \times 10^{-4} \text{ cm}^2 \text{ V}^{-1} \text{ s}^{-1}$  ( $n = 12$ ), as compared to  $3.3 \pm 0.2 \times 10^{-4} \text{ cm}^2 \text{ V}^{-1} \text{ s}^{-1}$  ( $n = 12$ ), for zwitterionic liposomes. This mobility difference is clearly caused by their electrophoresis running in opposite directions (Table 1), one against (in the case of DJLs) and the other along the same direction as the counter flow of EOF.

### Electrostatic self-assembly of DJLs

Unlike solid dipolar Janus particles, whose binding occurs exclusively *via* oppositely-charged hemispheres,<sup>10</sup> clustering of DJLs apparently occurs between both dissimilar (Fig. 4a–d) and similar domains (Fig. 4e–h). In the former case, the  $l_o$  and  $l_d$  domains were further found to join each other in either head-to-head (Fig. 4a and b), or head-to-side (Fig. 4c) or side-to-side (Fig. 4c) fashion, with the last configuration less frequently observed. On the other hand, liposome clustering *via* similar lipid domains was somewhat surprising, as it implies binding between like charges – a thermodynamically disfavored scenario.

To account for such unexpected formations, we consider here a pair of unique features associated with the current liposome system. (1) The presence of smaller lipid particles. As evident from Fig. 4b, g and h, these particles are also being produced by the hydration process alongside the micro-sized DJLs. Being charged and more mobile, these small particles often find larger liposomes to bind and, in doing so, can modify the surface charge composition of the latter. (2) Small lipid domains present in the “wrong” hemispheres, which can exist as kinetically trapped local states as a result of incomplete coalescence. As noted previously by other workers, these local

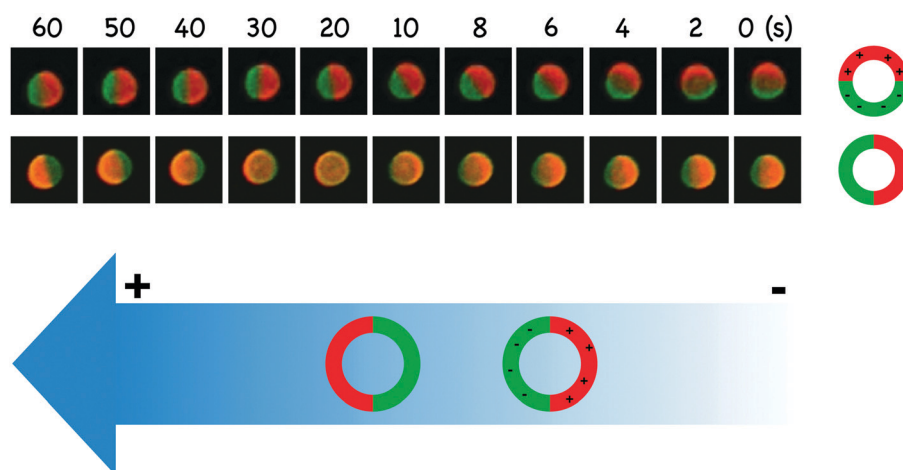


**Fig. 3** Characteristic rotation and alignment of individual dipolar (top row) and zwitterionic (second row) Janus liposomes in response to an electric field ( $1 \text{ V cm}^{-1}$ ). The numbers given at the top of the images indicate the time elapsed (in seconds) since the field was turned on at time 0. The movies from which these snapshots are taken can be found in the ESI.<sup>†</sup> (bottom) Schematic of the direction (indicated by the blue arrow) and relative mobility of liposome movement in relation to polarity of the applied field. Their domain-specific alignments with the field are also shown; both liposomes are  $\sim 11 \mu\text{m}$  in diameter.

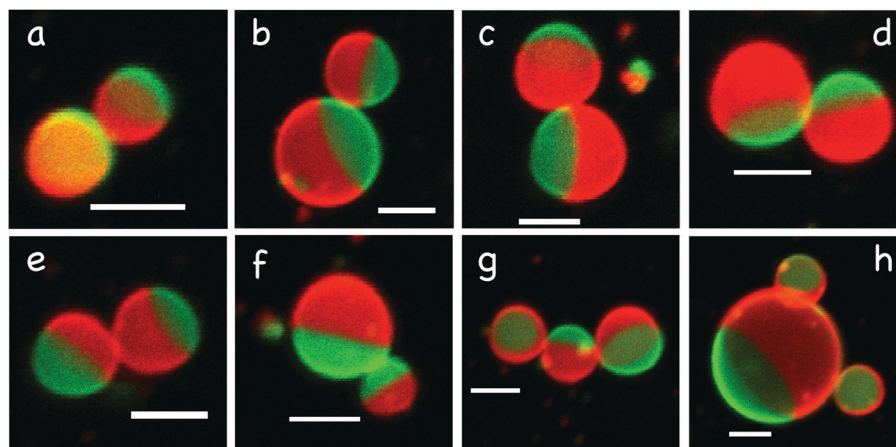


Fig. 4 DJL dimer (images a–f) and trimer (g and h) formation under a relatively low liposome density (total lipid concentration:  $\sim 1.25 \mu\text{M}$ ). Before imaging, these liposomes were incubated for 2 h at room temperature in the dark. Scale bar:  $10 \mu\text{m}$ .

states may persist in phase-separated lipid systems either due to high membrane viscosity<sup>15</sup> or interdomain repulsion.<sup>28</sup> Conceivably, the like charges present in these small domains add electrostatic repulsion between them, thus discouraging their merging even more.<sup>29</sup> Since these small domains bear the opposite charge of the hemispheres in which they are situated, they in effect serve as binding sites to link similar domains of DJLs in proximity.

When incubated at a relatively high liposome concentration, the increased number of DJLs present promotes more frequent liposome encounters and hence the formation of more extended clusters. A very informative sequence of images capturing such

assembling events is included in Fig. 5 (top section). At the beginning of this sequence, there are about a dozen separate DJLs sitting on the floor of the imaging chamber. Two pairs of dimers are formed in the first two minutes near the center of the view (marked by a broken circle), as these DJLs bind “head-to-head” with their neighbors just a few microns away. The close proximity between the two dimers allowed them to further approach each other to make contact in the next few minutes – this time between  $l_d$  domains with the assistance of a smaller liposome, producing a tetramer. This tetramer was later joined by a third dimer coming from the lower left (marked by broken oval, 8 min), and the new contact appears to be between  $l_o$  domains.

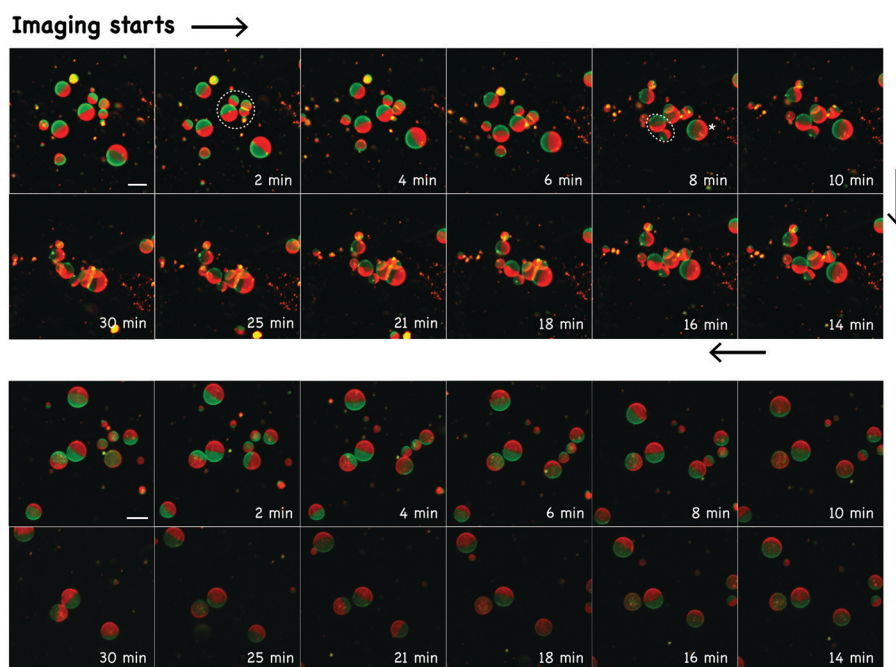


Fig. 5 (top) Time-sequenced fluorescence micrographs of DJLs undergoing aggregation. Liposomes are imaged right after their formation; total lipid concentration:  $5 \mu\text{M}$ . (bottom) A similar sequence recorded for zwitterionic Janus liposomes (lipid composition: DPPC/DOPC/Chol/Bodipy-chol/Rho-DOPE, 40/40/20/0.2/0.2) as a control. Scale bar:  $20 \mu\text{m}$ .

Not too far behind, there is also another larger liposome (marked by asterisk, 8 min) approaching the tetramer from the right side. Since the size/orientation of this newcomer's  $l_o$  domain matched well with the  $l_d$  domain of the tetramer, they bound and subsequently fused into each other (16 and 18 min). This interaction is so powerful that it appears to cause the third dimer to detach from the tetramer (21 to 30 min). Intriguingly, prior to its merging, this (bigger) liposome not only rolls directly toward its binding partner but at the same time, also rotates so as to achieve a favorable orientation for binding. Such “docking”-like movement is absent in electrostatic binding between homogeneous anionic/cationic liposomes,<sup>30,31</sup> and once again confirms the dipolar charge configuration in these liposomes.

A drastically different interaction behavior was displayed by Janus liposomes bearing no DPPG or DOTAP. With a comparable liposome density to start with, these particles diffuse around and would temporarily get so close to each other to appear in direct contact, but always part their ways afterwards (Fig. 5, bottom section). Clearly, being in close proximity alone is insufficient for the two zwitterionic lipid bilayers to initiate fusion. Since lipid fusion involves extensive lipid/water reorganization at the interfaces, some more forceful binding mechanism has to be in place to overcome the associated energy barriers. In cell biology, for example, this task is often fulfilled by the soluble *N*-ethylmaleimide-sensitive factor attachment protein receptor (SNARE)<sup>32</sup> complexes located on cargo vesicles and the target membrane. There, interestingly, electrostatic attraction is also found to play a central role in complementary binding between SNARE complexes, a process facilitated specifically by protein motifs enriched with cationic lysine and anionic glutamic acid residues.<sup>33</sup>

Above we have demonstrated that anionic/cationic lipids as minor components can be selectively sorted into the two immiscible liquid domains of the DPPC/DOPC/cholesterol system to yield dipolar Janus liposomes. Underlying such preferential phase partitioning is the mismatched acyl chains of these charged lipids, dipalmitoyl (16:0) *vs.* dioleoyl (18:1), whose mixing into dissimilar lipid domains would greatly disrupt the preferred lipid packing and motion therein and thus skyrocket the potential energy of the system. This energy penalty, for example, amounts to about  $2k_B T$  per lipid<sup>16</sup> for DOPC mixed with DPPC and cholesterol at room temperature, which the system elects to avoid by undergoing phase separation. On the other hand, electrostatic interactions among charged lipids, *i.e.*, both like-charge repulsion (in the same domain) and opposite-charge attraction (between dissimilar domains), are expected to be present to oppose such lipid phase separation. Theoretically, these electrostatic interactions appear to be strong enough to dominate the energy landscape, *e.g.*,  $\sim 6k_B T$  per charge, according to the Poisson–Boltzmann model.<sup>34,35</sup> If so, why does phase separation of DPPG/DOTAP still occur in these DJLs?

Working with several ternary lipid systems containing cholesterol together with diphytanoyl (low-melting) and dipalmitoyl (high-melting) lipids, Keller and coworkers found that addition of anionic PG lipids (to replace PCs of identical acyl chains), even up to 60%, only has a minimal influence on

the primary phase separation of the system.<sup>36</sup> To account for similarly dominating charge repulsion, these authors suggested several possible scenarios where the negative charge might be compensated, such as ion condensation and H-bonding between PG lipids. The former possibility can be more quantitatively assessed in our case as follows. Assuming complete ionization, 2% DPPG located in the  $l_o$ -half of a Janus liposome roughly corresponds to a surface charge density ( $\sigma$ ) of  $5 \times 10^{-3} \text{ C m}^{-2}$ .<sup>37</sup> Following, then, the Grahame equation,<sup>39,40</sup>  $\sigma = (8\epsilon_0\epsilon k_B T)^{1/2} \sinh(e\psi_0/2k_B T) C_{\text{mono}}^{1/2}$ , where  $\psi_0$  is the surface potential,  $C_{\text{mono}}$  the concentration of monovalent supporting electrolyte and the rest carrying their conventional meaning/value, we obtain  $\psi_0$  at about  $-0.3 \text{ V}$ , which is much greater than the measured zeta potential ( $-19.1 \text{ mV}$ , Table 1). Because zeta potential reports the potential imparted by a charged particle plus its associated counter ions within its surface of shear,<sup>26</sup> it becomes clear that the majority of the supporting ions are condensed on the surface of the liposome. A similar conclusion can be drawn for DOTAP-doped liposomes.

Such ion condensation, however, can only offset the electrostatic interactions for so long. As the percentage of charged lipids increases, the latter will increase in magnitude, eventually dominating the energetics in the system. This shift of dominance can be seen, for example, when 10% DPPG/DOTAP each were added into the formation (ESI,† Fig. S2a). While liposomes were still being produced with a good yield at this high doping level, very few of them possess the desired Janus configuration, which is likely due to compromised lipid phase separation caused by strong electrostatic interactions. At the intermediate doping level of 5%, by contrast, Janus liposome formation remains feasible (ESI,† Fig. S2b). Taken together, these results point to the existence of an upper limit on the amount of oppositely charged lipids that can be sorted into immiscible liquid/liquid lipid domains. In addition to the charge doping level, this limit is expected to also depend on other factors, such as the structure and mixing ratio of charged lipids and host lipids.

Another interesting finding of this work is the nonuniform, domain-specific electrostatic binding displayed by DJLs. While oppositely charged nanospheres bind the DOTAP-residing  $l_d$  domain evenly and fully given enough time, the nanosphere coverage on the DPPG-occupied  $l_o$  domain remains dotted and discontinuous (Fig. 2). Such discreteness cannot be attributed entirely to the different charge density carried by the two types of nanospheres (Table 1), which would only alter the extent of their attachment, but not their location or binding pattern, on liposomes. Rather, it is the structural dissimilarity between DOTAP and DPPG, as well as the different lipid environments in which they are situated, that are directly responsible for the observed contrasts. Owing to their phosphate and glycerol groups, DPPG hydrogen bonds extensively with neighboring lipids as well as water molecules, which in turn causes its tight packing in bilayers, *e.g.*, an area of  $0.48 \text{ nm}^2$  occupied per lipid,<sup>41</sup> as compared to  $0.73 \text{ nm}^2$  for DOTAP<sup>41</sup> or  $0.64 \text{ nm}^2$  for DPPC.<sup>42</sup> To the aqueous-suspended nanospheres, this structural arrangement of DPPG poses a constraint not only on the



binding accessibility, but also on its efficiency. Complicating the matter further are the  $l_o$  vs.  $l_d$  domains hosting DPPG and DOTAP, which represent two drastically different lipid environments,<sup>43–45</sup> e.g., in lipid packing density, lateral mobility and hydration level. To evaluate the impact of these factors with any certainty, further work is clearly needed.

## Summary

Above we have presented a lipid-sorting based scheme to prepare dipolar Janus liposomes and fluorescence microscopic characterization of their electrokinetic motion and electrostatic self-assembly. Together with the evidence from nanosphere binding analysis, these results establish that these liposomes bear simultaneously broken surface symmetry and opposite surface charges on the same colloidal body. This unique molecular assembly formation may be of fundamental interest in the areas of lipid colloid chemistry and self-assembly and moreover adds an all-lipid-based soft material into the fast-growing inventory of patchy particles.

## Conflicts of interest

There are no conflicts to declare.

## Acknowledgements

This work is supported by the National Science Foundation (award No. CHE-1808123). We thank Prof. Dongye Zhao for his assistance in zeta potential measurement.

## References

- 1 A. Perro, S. Reculosa, S. Ravaine, E. Bourgeat-Lami and E. Duguet, *J. Mater. Chem.*, 2005, **15**, 3745–3760.
- 2 S. Jiang, Q. Chen, M. Tripathy, E. Luijten, K. S. Schweizer and S. Granick, *Adv. Mater.*, 2010, **22**, 1060–1071.
- 3 A. Walther and A. H. E. Müller, *Chem. Rev.*, 2013, **113**, 5194–5261.
- 4 G. Loget and A. Kuhn, *J. Mater. Chem.*, 2012, **22**, 15457–15474.
- 5 X. Pang, C. Wan, M. Wang and Z. Lin, *Angew. Chem., Int. Ed.*, 2014, **53**, 5524–5538.
- 6 A. Kirillova, C. Marschelke and A. Synytska, *ACS Appl. Mater. Interfaces*, 2019, **11**, 9643–9671.
- 7 P. Akcora, H. Liu, S. K. Kumar, J. Moll, Y. Li, B. C. Benicewicz, L. S. Schadler, D. Acehan, A. Z. Panagiotopoulos, V. Pyamitsyn, V. Ganesan, J. Ilavsky, P. Thiyagarajan, R. H. Colby and J. F. Douglas, *Nat. Mater.*, 2009, **8**, 354–359.
- 8 M. S. Nikolic, C. Olsson, A. Salcher, A. Kornowski, A. Rank, R. Schubert, A. Frömsdorf, H. Weller and S. Förster, *Angew. Chem., Int. Ed.*, 2009, **48**, 2752–2754.
- 9 S. Jiang, M. J. Schultz, Q. Chen, J. S. Moore and S. Granick, *Langmuir*, 2008, **24**, 10073–10077.
- 10 L. Hong, A. Cacciuto, E. Luijten and S. Granick, *Nano Lett.*, 2006, **6**, 2510–2514.
- 11 P. A. Beales, J. Nam and T. K. Vanderlick, *Soft Matter*, 2011, **7**, 1747–1755.
- 12 M. Wang, Z. Liu and W. Zhan, *Langmuir*, 2018, **34**, 7509–7518.
- 13 M. J. Sarmiento, M. Prieto and F. Fernandes, *Biochim. Biophys. Acta*, 2012, **1818**, 2605–2615.
- 14 N. Momin, S. Lee, A. K. Gadok, D. J. Busch, G. D. Bachand, C. C. Hayden, J. C. Stachowiak and D. Y. Sasaki, *Soft Matter*, 2015, **11**, 3241–3250.
- 15 S. L. Veatch and S. L. Keller, *Biophys. J.*, 2003, **85**, 3074–3083.
- 16 S. L. Veatch, I. V. Polozov, K. Gawrisch and S. L. Keller, *Biophys. J.*, 2004, **86**, 2910–2922.
- 17 J. H. Davis, J. J. Clair and J. Juhasz, *Biophys. J.*, 2009, **96**, 521–539.
- 18 H. M. McConnell and M. Vrljic, *Annu. Rev. Biophys. Biomol. Struct.*, 2003, **32**, 469–492.
- 19 T. Nisisako, T. Torii, T. Takahashi and Y. Takizawa, *Adv. Mater.*, 2006, **18**, 1152–1156.
- 20 G. Okano and T. Akino, *Lipids*, 1979, **14**, 541–546.
- 21 A. E. Regelin, S. Fankhaenel, L. Gürtesch, C. Prinz, G. von Kiedrowski and U. Massing, *Biochim. Biophys. Acta*, 2000, **1464**, 151–164.
- 22 E. Maltseva, V. L. Shapovalov, H. Möhwald and G. Brezesinski, *J. Phys. Chem. B*, 2006, **110**, 919–926.
- 23 C. Chen and C. P. Tripp, *Biochim. Biophys. Acta*, 2012, **1818**, 1673–1681.
- 24 C. Bonechi, S. Martini, L. Ciani, S. Lamponi, H. Rebmann, C. Rossi and S. Ristori, *PLoS One*, 2012, **7**, e41438.
- 25 O. Gustafsson, K. B. Mogensen and J. P. Kutter, *Electrophoresis*, 2008, **29**, 3145–3152.
- 26 R. J. Hunter, *Zeta Potential in Colloid Science*, Academic Press Inc., London, UK, 1981.
- 27 N. L. Burns, J. M. Van Alstine and J. M. Harris, *Langmuir*, 1995, **11**, 2768–2776.
- 28 M. Yanagisawa, M. Imai, T. Masui, S. Komura and T. Ohta, *Biophys. J.*, 2007, **92**, 115–125.
- 29 C. C. Vequi-Suplicy, K. A. Riske, R. L. Knorr and R. Dimova, *Biochim. Biophys. Acta*, 2010, **1798**, 1338–1347.
- 30 D. P. Pantazatos and R. C. MacDonald, *J. Membr. Biol.*, 1999, **170**, 27–38.
- 31 F. M. Menger, J. S. Keiper and S. J. Lee, *Langmuir*, 1997, **13**, 4614–4620.
- 32 T. C. Südhof, *Annu. Rev. Neurosci.*, 2004, **27**, 509–547.
- 33 S. Wagle, V. N. Georgiev, T. Robinson, R. Dimova, R. Lipowsky and A. Grafmüller, *Sci. Rep.*, 2019, **9**, 7708.
- 34 D. F. Evans and H. Wennerström, *The Colloidal Domain*, Wiley-VCH, New York, 2nd edn, 1999.
- 35 D. H. Mengistu and S. May, *J. Chem. Phys.*, 2008, **129**, 121105.
- 36 M. C. Blosser, J. B. Starr, C. W. Turtle, J. Ashcraft and S. L. Keller, *Biophys. J.*, 2013, **104**, 2629–2638.
- 37 This value is estimated geometrically with the following additional assumptions: (1) all DPPGs are located in the  $l_o$  hemisphere, together with (2) DPPC/DOPC and cholesterol mixed at 7:3 mole ratio (taken from ref. 38) and (3) all lipids occupy the same area per lipid as in their respective single-component bilayers. The detail of this calculation is given in the ESI†.
- 38 S. L. Veatch, O. Soubias, S. L. Keller and K. Gawrisch, *Proc. Natl. Acad. Sci. U. S. A.*, 2007, **104**, 17650–17655.



- 39 D. C. Grahame, *Chem. Rev.*, 1947, **41**, 441–501.
- 40 J. N. Israelachvili, *Intermolecular and Surface Forces*, Elsevier Inc., Amsterdam, The Netherlands, 3rd edn, 2011.
- 41 W. Zhao, A. A. Gurtovenko, I. Vattulainen and M. Karttunen, *J. Phys. Chem. B*, 2012, **116**, 269–276.
- 42 S. W. Chiu, E. Jakobsson, R. J. Mashl and H. L. Scott, *Biophys. J.*, 2002, **83**, 1842–1853.
- 43 T. Róg, M. Pasenkiewicz-Gierula, I. Vattulainen and M. Karttunen, *Biochim. Biophys. Acta*, 2009, **1788**, 97–121.
- 44 P. Heftberger, B. Kollmitzer, A. A. Rieder, H. Amenitsch and G. Pabst, *Biophys. J.*, 2015, **108**, 854–862.
- 45 Y. Ma, S. K. Ghosh, D. A. DiLena, S. Bera, L. B. Lurio, A. N. Parikh and S. K. Sinha, *Biophys. J.*, 2016, **110**, 1355–1366.